Journal of Materials Chemistry A

Accepted Manuscript

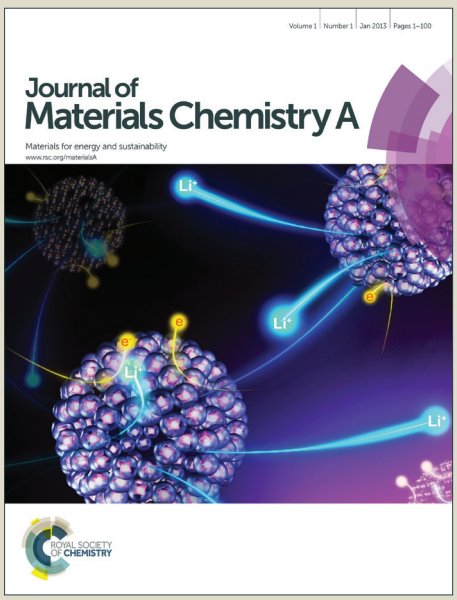

ROYAL SOCIETY OF CHEMISTRY

www.rsc.org/materialsA

Journal of Materials Chemistry A RSCPublishing

Paper

Approaching the theoretical capacitance of graphene through copper foam integrated three-dimensional graphene networks

Cite this: DOI: 10.1039/x0xx00000x

Received 00th January 2015,
Accepted 00th January 2015

DOI: 10.1039/x0xx00000x

www.rsc.org/

Ramendra Sundar Dey,[a] Hans A. Hjuler[b] and Qijin Chi[a]*

We report a facile and low-cost approach for the preparation of all-in-one supercapacitor electrodes using copper foam (CuF) integrated three-dimensional (3D) reduced graphene oxide (rGO) networks. The binder-free 3DrGO@CuF electrodes are capable of delivering high specific capacitance approaching to the theoretical capacitance of graphene and exhibit high charge-discharge cycling stability.

As a new carbon allotrope, graphene holds promise for development of electrochemical double layer (EDL) capacitors, due to its large specific surface area (with a theoretical specific surface area of 2630 m^2 g^{-1}), high conductivity, chemical stability, low-cost and feasibility of large-scale production.[1] Moreover, the high mechanical strength and flexibility of this atomically-thin two-dimensional carbon allotrope makes graphene particularly conspicuous to fabricate light, flexible and binder-free supercapacitors.[2,1a] Even though graphene possesses these advantages, graphene-based supercapacitors still have not reached the theoretical capacitance as high as ~550 F g^{-1} due to self-aggregation or re-stacking of graphene sheets.[3] Doping graphene with electroactive capacitive materials (e.g. MnO_2, RuO_2, Co_3O_4, polyaniline) enables to construct pseudo-supercapacitors with high specific capacitances (200-1000 F/g).[4] On the other hand, inefficient ionic and electronic transport of pseudo- capacitive material-based electrodes often causes specific capacitance fading rapidly over charge-discharge cycling, particularly at high charging/discharging speeds. This is a major setback for the use of graphene-based materials in supercapacitors.[5] Recently, 3D graphene networks have been studied as a possible solution.[3,6] However, most studies have shown that specific capacitance is not as high as expected or high specific capacitance is achieved only with charge/discharge at low current densities (<1 A/g) or at low potential scan rates (<50 mV/s). A major cause is attributed to significant π-π re-stacking of graphene sheets during material preparation, assembly and charge-discharge processes, leading to insufficient pore size for access of electrolytes.[7] Therefore, it is highly desirable to develop a binder-free, self-supported integrated system for construction of 3D porous graphene based high-performance supercapacitor. The present work is motivated towards such a goal.

Two major technical challenges (or limitations) in the use of 3DrGO materials for supercapacitors are: 1) 3DrGO is mechanically fragile and its electrical conductivity is practically low, 2) attachment (or transfer) of 3DrGO networks to a current collector with *low contact resistance* and *without destroying 3D structures* is another considerable challenge. The latter would be of crucial limitation in practical use of 3DrGO-based materials for supercapacitors, even if they possess large specific surface area. This work has demonstrated a facile and low-cost

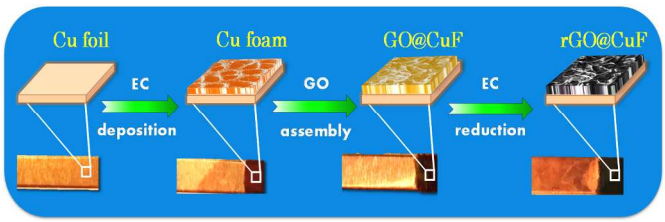

Scheme 1. Schematic representation of the overall procedure for the stepwise fabrication of 3DrGO@CuF electrode materials. Digital pictures of the resulting electrode materials at different stages are shown in the bottom row.

[a] Department of Chemistry, Technical University of Denmark, DK-2800 Kongens Lyngby, Denmark.
E-mail: cq@kemi.dtu.dk; Phone: +45 45252032; Fax: +45 45883136.
[b] Danish Power Systems, Dreyersvej 30, 2960 Rungsted Kyst, Denmark.

† Electronic Supplementary Information (ESI) available: the details of materials and methods, additional microscopic images and electrochemical data. See DOI: 10.1039/c000000x/

strategy to prepare 3DrGO on copper foam (CuF), with the aim at the cost-effective fabrication of all-in-one supercapacitor electrodes with large effective contact areas and high cycling performances, leading to approaching to the theoretical capacitance of graphene. Recently, there are some reports related to Cu supported graphene material based supercapacitor electrodes, but their performances are needed to be further improved.[8] To the best of our knowledge, this is the first attempt of using CuF as both a template for assembly of 3DrGO and a current collector for supercapacitors. The resulting binder-free supercapacitor electrodes show substantial energy density and high cycling stability also.

The overall procedure for the preparation of 3DrGO on CuF is illustrated schematically in Scheme 1. Digital photos of resulting electrode materials obtained at different stages are shown in the bottom row in Scheme 1 and Fig. S1 ESI†. Electrochemical reduction was performed to convert self-assembled GO to rGO (Fig. S2 ESI†). The morphology and structures of the rGO@CuF hybrid material were characterized systematically by field-emission gun scanning electron microscope (FEG-SEM) and AFM. The surface structure of Cu foil before and after the deposition of CuF was imaged by FEG-SEM, and the representative images are compared in Figure S3 (ESI†). Figure 1 shows typical SEM images of 3DrGO@CuF hybrid materials deposited on CuF, by which three types of structures in different locations are clearly revealed. Figure 1a-1c shows the structure of 3DrGO on the boundary of CuF, which is the porous graphene network consisting of interconnected nanosheets. Figure 1d-1f shows the structure of the 3DrGO inside the CuF pore, and Figure 1g-1i shows the structure of 3DrGO at the wall of the CuF pore. High-resolution SEM images (Figure 1c, 1f and 1i) suggest that, the attachment of GO sheets does not change the frame structure of CuF but GO nanosheets self-assembles into hierarchically porous structures using CuF as the template and support. The detailed structures of 3DrGO@CuF clearly show that the material possess large effective contact area. The partial overlapping (or linking) of rGO sheets leads to the formation of a 3D porous network. The interconnection is driven most likely by different types of interactions between graphene nanosheets, including van der Waals attraction, hydrogen bonding via oxygen-containing groups at sheet edges and partial π-π stacking.[9]

It is noticed that the structure of 3DrGO is also dependent on the CuF pore size, thickness and the GO loading amount. We have prepared Cu foams with various pore sizes ranging from 80 to 120 μm by changing the electrodeposition time (Fig. S4 ESI†). The average size of pores in CuF is determined from the size-distribution histograms (Fig. S5 ESI†). The thickness of the CuFs prepared by 40, 50 and 60s electrodeposition time are 100, 125 and 150 μm, respectively (Fig. S4c, 4f and 4i ESI†). The Cu foams with the pore size of ≈120 μm (Fig. S6 ESI†) show the best suitability for self-assembly of GO nanosheets to form high-performance 3DrGO networks. It is clear from the Figure S7 (ESI†) that the 0.08 mg/cm^2 is the optimized loading amount for GO to form porous networks which fully covered the CuF without significant stacking. The increased amount of GO results in aggregation and blocks the porous structure of both 3DrGO and CuF (Fig. S7c-7e ESI†).

AFM was used to further disclose the structural features of 3DrGO@CuF samples. High-resolution AFM images enable to offer more details of the structural features. Similar to SEM observations, AFM *first* reveals that rGO sheets maintain 3D network structures of CuF throughout all prepared samples and are partially stacked in some regions interconnected to form 3D framework (Figure 2a-2d). More details are also revealed that rGO sheets are crumpled and tightly cover CuF pores over the whole surface of CuF (Fig. 2a-2b). This observation suggests that there is strong adhesion between rGO sheets and Cu substrate. It is also noted that similar AFM images of GO@CuF (Fig. S8 ESI†) and rGO@CuF (Figure 2a-2b) demonstrate that the 3D structural integrity does not alter by electrochemical reduction. The Real surface areas of 3DrGO@CuF material was measured by electrochemical approach generally used for porous metal electrodes.[10] We used popular voltammetry approach to estimate the effective surface areas of the 3DrGO@CuF materials (see ESI†) and is found to be 1000 m^2/g (Fig. S9 ESI†).

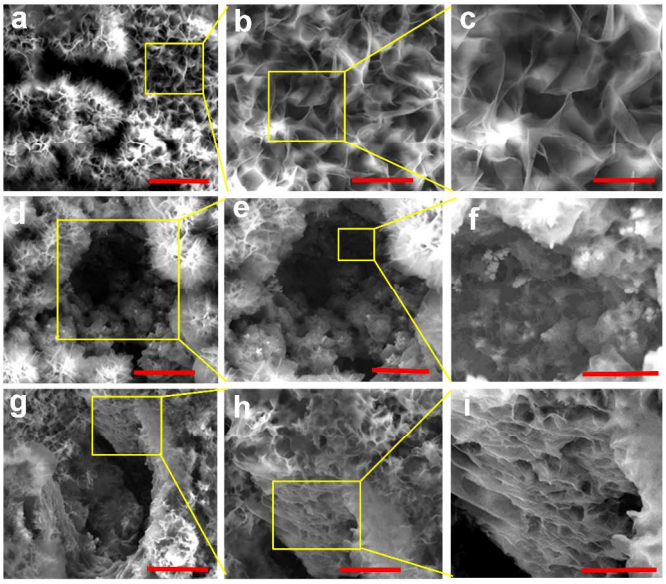

Figure 1. Microscopic characterization of three-type structures. SEM Images of (a-c) 3DrGO at the boundary of CuF, (d-f) 3DrGO inside the pore of CuF and (g-i) 3DrGO on the wall of CuF. The scale of bars: (a) 50 μm, (b) 10 μm, (c) 5 μm, (d) 50 μm, (e) 20 μm, (f) 10 μm, (g) 50 μm, (h) 20 μm and (i) 10 μm.

GO@CuF and rGO@CuF hybrid materials were analyzed by X-ray diffraction (XRD) (Fig. S10 ESI†). The XRD patterns reveal that the typical diffraction peak of GO at 2θ = 9.1° disappears in rGO@CuF samples due to removal of oxygen-containing functional groups from GO planes by electrochemical reduction. Furthermore, the graphite diffraction peak is not observed for rGO@CuF, a clear indication that electrochemical reduction did not cause re-stacking of rGO sheets into graphite. This observation is consistent with those obtained from AFM and SEM images, i.e. the overall 3D network structures are retained after electrochemical reduction.[11]

As the material is highly porous, thin, conductive and possess good electrical contact interfaces, 3DrGO@CuF is a promise material for supercapacitor electrodes. The potential of this material for supercapacitors has been tested systematically by the so-called best-practice methods using cyclic voltammetry and galvanostatic charge-discharge measurements. Figure 3a shows a cyclic voltammogram (CV) of rGO@CuF electrodes at a scan rate of 0.1 V s^{-1}. Rectangular-like, horizontal, largely symmetric features in CV indicate that rGO@CuF electrodes have ideal EDL capacitive nature and good charge propagation in the potential window of -0.2 V to -0.8 V. Large capacitive currents result from high specific area of rGO@CuF electrodes and high conductivity. The CVs

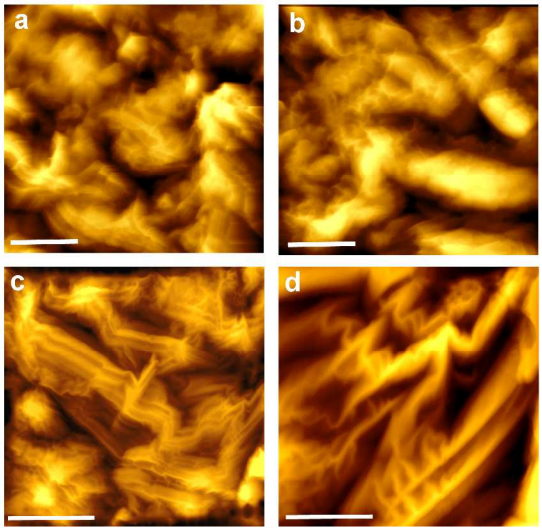

Figure 2. High-resolution microscopic structures. AFM (a-b) Images of 3DrGO-CuF on Cu supports. (c-d) are the high-resolution images. The scale of bars: (a) 5 µm, (b) 5 µm, (c) 2 µm and (d) 0.5 µm

obtained at different scan rates are compared (Fig. S11 ESI†). With increasing scan rate, the capacitive current increases but the symmetric rectangular shape is largely retained only with a slight distortion at high scan rates. This observation suggests that 3DrGO@CuF electrodes have high capacitive performance and small internal resistance of 3DrGO at the CuF surfaces and interfaces. It is important to note that the amount of GO self-assembled on CuF and the pore size of CuF have significant impacts on the specific capacitance (C_{sp}) of 3DrGO@CuF. The voltammetric and charge-discharge behaviour of 3DrGO@CuF with different loadings of GO was evaluated (Fig. S12 ESI†). The C_{sp} was calculated from charge-discharge curve, and it was observed that 0.08 mg/cm^2 of GO on CuF contribute highest specific capacitance (Table S1 ESI†). The specific capacitance decreases with increasing GO loading. The SEM micrograph (Fig. S4 ESI†) shows that increasing GO loading affects the porous structure, leading to the formation of aggregated structure when the GO loading was larger than 0.4 mg/cm^2. We have also evaluated the effects of the CuF pore size on the C_{sp} of 3DGO@CuF material. The 3DGO@CuF electrodes with different pore size of CuF was synthesized by changing electrodeposition time but keeping the same loading amount of GO at 0.08 mg/cm^2. The CVs and charge-discharge curves were recorded with those materials (Fig. S13 ESI†). The 3DrGO@CuF electrodes with an average pore size of ≈120 µm (i.e. 60s electrodeposition) give rise to the best performance (Table S1 and Fig. S13 ESI†). This observation can be explained by the structural characteristics revealed by SEM. As shown by the SEM images (Fig. S5 ESI†), the CuF with the pore size of ≈120 µm is well covered with rGO layers to form an open porous 3D network. In addition, we have also synthesized the CuF with the pore size larger than 120 µm by increasing electrodeposition time. However, the as-synthesized thicker CuFs are not stably retained but often detached from the Cu foil bulk.

The capacitive performance of rGO@CuF electrodes was further investigated with galvanostatic charge/discharge cycles. Figure 3b and Fig. S14 (ESI†) show charge/discharge curves of rGO@CuF electrodes at different applied current densities ranging from 1 to 100 A g^{-1}. The C_{sp} of the material was calculated from the discharging curves and is plotted vs current density (Figure 3c). The C_{sp} of rGO@CuF electrodes at 1 A g^{-1} can reach 623 ± 7 F g^{-1}, which is among the highest specific capacitance reported for 3DrGO based materials.[5a,6,7,12] However, the observed capacitance is contributed not only by 3DrGO but also from CuF itself as discussed below. As expected, the C_{sp} decreases with increasing current density. However, the specific capacitance is still high even at high current densities. For instance, the material retained its C_{sp} at 416 F g^{-1} with 10 A g^{-1} applied (i.e. 67% retained with respect to that obtained at 1 A g^{-1}) and 317 F g^{-1} at 100 A g^{-1} (i.e. 51% retained). There is no *IR* drop observed at high current densities (5 to 100 A g^{-1}) on the discharge curves and very small *IR* drop observed at low current densities (1 to 2 A g^{-1}). This observation indicates that the electrodes have a small internal resistance, consistent with the conclusion from voltammetric results (Figure 3a). In addition, one interesting feature is noted that rGO@CuF electrodes show excellent cycling performance (2000 continuous cycles) even at a high current density such as 10 A g^{-1} (Figure 3d). Symmetrical and triangular charge/discharge curves observed indicate low mass transfer resistance and good charge propagation of electrolyte ions in the porous 3DrGO networks, which is highly desirable for an ideal supercapacitor.[13] A slight enhancement in C_{sp} is observed up to the first 500 cycles (i.e. from 416 increased to 430 F g^{-1}, Fig 3e) which is likely due to initial activation of the material, and after that the capacitance keeps largely constant in the following cycles. After 2000 cycles, the C_{sp} value reduced slightly to 425 F g^{-1} but with still ~99% retention of C_{sp} with respect to the steady C_{sp} (430 F g^{-1}) after 500 cycles, indicate the electrodes possess good cycling stability and a high degree of reversibility. Following cycling stability measurements, the system durability was checked by cyclic voltammetry. Clearly, there is no detectable decay in voltammetric responses after 2000 cycles (Fig. S15 ESI†), suggesting that the structural integrity is retained. To further confirm the structural feature after cycling, we checked the SEM images before and after cycling. It is clear from the SEM images (Fig. S16 ESI†) that the structure of 3DGO@CuF material does not change its integrity after 2000 charge-discharge cycles.

To clarify the contributions of Cu components (including bulk Cu and Cu foam) and GO to the high specific capacitance (623 F g^{-1}) observed, the control experiments with CuF and 3DGO@CuF as supercapacitor electrodes were performed in parallel. Their CVs and charge-discharge curves were recorded and are compared to those for rGO@CuF (Fig. S17 ESI†). The C_{sp} of CuF and GO@CuF is 20 F g^{-1} and 234 F g^{-1}, respectively, about 30 and 3 times lower than that for rGO@CuF electrodes. Therefore, while GO@CuF can also be used as supercapacitor electrodes, but the electrochemical conversion of GO into rGO is essential for enhancing performance in the present case. In the case of CuF alone, the initial capacitance was very small (only 20 F g^{-1}). However, we noticed that upon further charge-discharge cycling at a fixed current density (e.g. 1 A g^{-1}) the specific capacitance of CuF increased continuously up to 1000 cycles (Fig. S18 ESI†). The specific capacitance obtained after 1000 cycles was 110 F g^{-1}, which was stable up to 1700 cycles then decreased.

It is reported that the quantum capacitance of graphene can reach up to 21 µF cm^{-2},[14] which is equivalent to ~550 F g^{-1} by assuming all the specific surface areas (2630 m^2 g^{-1}) fully effectively used. As the contribution from CuF is 110 F g^{-1}, the specific capacitance contributed by 3DrGO is approximately 513 F g^{-1} i.e. over 90% of the theoretical value. This estimate does not cover possible cooperative contributions from the two

components, rGO and Cu foam. On the other hand, the results do show that this hybrid integrated system can generate high specific capacitance arising from optimal assembly and likely synergic interactions between rGO and CuF.

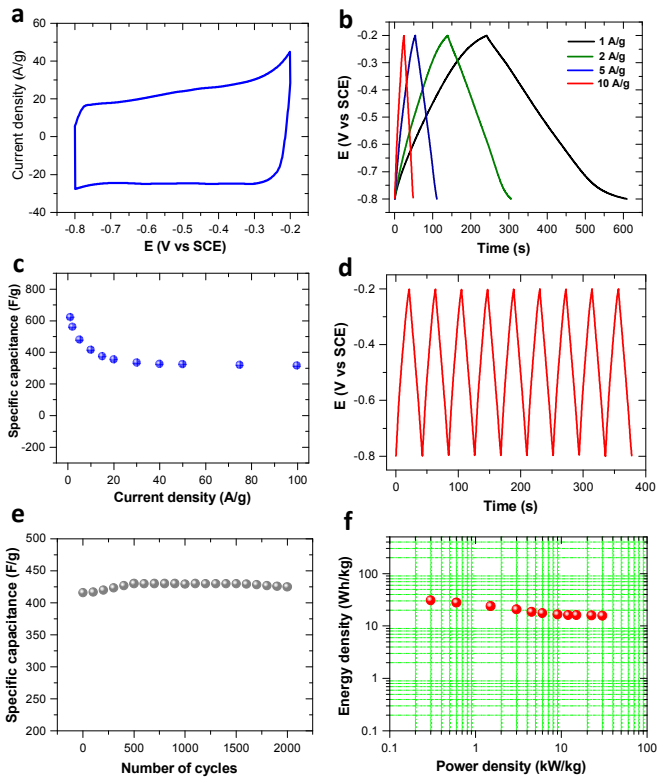

Figure 3. Supercapacitive performance of 3DrGO@CuF electrodes in PBS. (a) Cyclic voltammogram obtained with a scan rate of 100 mV s^{-1}. (b) Comparison of charge-discharge curves obtained at different current density. (c) Dependence of specific capacitance on applied current density. (d) Successive charge-discharge cycles at a current density of 10 A g^{-1}. (e) Change of specific capacitance over the charge-discharge cycles. (f) Typical Ragone plot for the present system.

Electrochemical impedance spectroscopy (EIS) was used to reveal the possible mechanisms of fast ion diffusion behaviour in conducting porous films. EIS spectra were recorded at the open circuit potentials of the systems with the frequency range of 10^5 Hz to 0.1 Hz and an amplitude of 10 mV applied and compared for different systems (Fig. S19 ESI†). The Nyquist plot of 3DrGO@CuF electrodes features a vertical curve almost parallel to the Y-axis (black dots in Fig. S19 ESI†), indicating that fast difussion and propagation of ions within the porous framework. In the high frequency region, the curves intersect the real axis approximately at 45° angle (the inset in Fig. S19 ESI†) signifies fast kinetics of ion transfer, which is an advantageous feature for a porous electrode when saturated with electrolyte.[12c]

The Ragone plot of the present system, which is a characteristic indication of both energy density and power density, is shown in Figure 3f. The maximum energy density of 31 Wh/kg is achieved with the power density of 0.3 kW/kg. The maximum power density of 30 kW/kg is obtained with the energy density of 16 Wh/kg. The energy density is significantly higher than most reported values to date for pure porous graphene–based materials in the literature[5b,6a,12a-b].

In conclusion, Cu foam serves an effective framework for self-assembly of three-dimensional GO networks that can be converted into rGO by electroreduction, and the Cu substrate acts as an excellent current collector. The overall procedure enables us to fabricate all-in-one supercapacitor electrodes with integrated 3DrGO networks as major capacitive species. Resulting 3DrGO@CuF electrodes have small internal resistance and exhibit high specific capacitance and cycling stability. Furthermore, the high-performance is achieved in environmentally friendly neutral solutions instead of commonly used strong acidic or basic solutions as well as with a relatively narrow potential window applied. The present system thus holds a great potential to be further enhanced in supercapacitive performance, for example by extension of its potential windows in organic media or/and ion liquids. Among others, such a detailed study is underway.

This work was supported financially by the Danish Research for Technology and Product Science (Project No. 12-127447). R.S.D. acknowledges the Hans C. Ørsted Postdoc Fellowship honoured by Technical University of Denmark. The authors thank the Kenny Ståhl group at DTU Chemistry for assistance in the XRD measurements.

Notes and references

1 (*a*) Y. Sun, Q. Wu and G. Shi, *Energy Environ. Sci*. 2011, **4**, 1113; (*b*) Y. Zhu et al., *Adv. Mater*. 2010, **22**, 3906; (*c*) R. S. Dey, S. Hajra, R. K. Sahu, C. R. Raj and M. K. Panigrahi, *Chem. Commun*., 2012, **48**, 1787.

2 Y. Zhu, et al. *Science* 2011, **332**, 1537.

3 H. Huang, L. Xu, Y. Tang, S. Tang and Y. Du, *Nanoscale*, 2014, **6**, 2426.

4 (*a*) Z.-S.;Wu, D.-W. Wang, W. Ren, J. Zhao, G. Zhou, F. Li and H.-M. Cheng, *Adv. Funct. Mater*. 2010, **20**, 3595. (*b*) S. Chen, J. Zhu, X. Wu, Q. Han and X.Wang, *ACS Nano* 2010, **4**, 2822; (*c*) Q. Wu, Y. Xu, Z. Yao, A. Liu and G. Shi, *ACS Nano* 2010, **4**, 1963;

5 (*a*) W. Wei, X. Cui, W. Chen and D. G. Ivey, *Chem. Soc. Rev*. 2011, **40**, 1697; (*b*) D. Bélanger, T. Brousse and J. W. Long, *Electrochem. Soc. Interface* 2008, **17**, 49; (*c*) K. Gopalakrishnan, K. Moses, A. Govindaraj, C. N. R. Rao, *Solid State Commun*. 2013, **175-176**, 43; (d) K. Gopalakrishnan, A. Govindaraj, C. N. R. Rao, *J. Mater. Chem. A*, 2013, **1**, 7563.

6 (*a*) L. Zhang and G. Shi, *J. Phys. Chem*. C 2011, **115**, 17206; (*b*) Y. Xu, K. Sheng, C. Li and G. Shi, *ACS Nano* 2010, **4**, 4324 (*c*) S. Ye, J. Feng, and P. Wu, *ACS Appl. Mater. Interfaces* 2013, **5**, 7122; (*d*) L. Zhang, F. Zhang, X. Yang, G. Long, Y. Wu, T. Zhang, K. Leng, Y. Huang, Y. Ma, A. Yu and Y. Chen, *Scientific Reports*, 2013, **3**, 1408.

7 X. Cao, Z. Yin and H. Zhang, *Energy Environ. Sci*., 2014, **7**, 1850.

8 (*a*) K. Wang, X. Dong, C. Zhao, X. Qian, and Y. Xu, *Electrochim. Acta*. 2015, **152**, 433; (*b*) X. Dong, K. Wang, C. Zhao, X. Qian, S. Chen, Z. Li, H. Liu, and S. Dou, *J. Alloys Compd*. 2014, **586**, 745; (*c*) C. Zhao, S.-L. Chou, Y. Wang, C. Zhou, H.-K. Liu and S.-X. Dou, *RSC Adv*. 2013, **3**, 16597.

9 O. C. Compton, Z. An, K. W. Putz, B. J. Hong, B. G. Hauser, L. C. Brinson and S. T. Nguyen, *Carbon* 2012, **50**, 3399.

10 S. Trasatti and O. A. Petrii, *J. Electroanal. Chem*. 1992, **327**, 353.

11 (*a*) F. Liu, S. Y. Song, D. F. Xue and H. J. Zhang, *Adv. Mater*. 2012, **24**, 1089; (*b*) W. F. Chen, S. R. Li, C. H. Chen and L. F. Yan, *Adv. Mater*. 2011, **23**, 5679−5683.

12 (*a*) U. N. Maiti, J. Lim, K. E. Lee, W. J. Lee and S. O. Kim, *Adv. Mater*. 2014, **26**, 615; (*b*) Z. Lei, F. Shi and L. Lu, *ACS Appl. Mater. Interfaces* 2013, **5**, 9656; (*c*) C. M. Niu, E. K. Sichel, R. Hoch, D. Moy and H. Tennent, *Appl. Phys. Lett.* 1997, **70**, 1480.

13 (*a*) J. Yan, T. Wei, B. Shao, F. Ma, Z. Fan, M. Zhang, C. Zheng, Y. Shang, W. Qian and F. Wei, *Carbo*n 2010, **48**, 1731; (*b*) W.-W. Liu, X.-B. Yan, J.-W. Lang, C. Peng and Q.-J. Xue, *J. Mater. Chem*., 2012, **22**, 17245; (*c*) L. L. Zhang, X. Zhao, M. D. Stoller, Y. Zhu, H. Ji, S. Murali, Y. Wu, S. Perales, B. Clevenger, and R. S. Ruoff, *Nano Lett*. 2012, 12, 1806.

14 J. Xia, F. Chen, J. Li and N. Tao, *Nat. Nanotechnol*. 2009, **4**, 505.

The table of content graphics

A facile and cost-effective approach to fabricate all-in-one integrated supercapacitor electrodes is achieved with copper foam integrated three-dimensional reduced graphene oxide networks for approaching the theoretical capacitance of graphene. The electrodes show high-performance in specific capacitance, charging-discharging stability and energy and power density.